Mon. Not. R. Astron. Soc. **376,** 1635–1647 (2007) doi:10.1111/j.1365-2966.2007.11421.x

Angular power spectrum of gamma-ray sources for *GLAST*: blazars and clusters of galaxies

Shin'ichiro Ando,[1,2]★ Eiichiro Komatsu,[3] Takuro Narumoto[4] and Tomonori Totani[4]

[1]*Theoretical Astrophysics, California Institute of Technology, Pasadena, CA 91125, USA*
[2]*Kellogg Radiation Laboratory, California Institute of Technology, Pasadena, CA 91125, USA*
[3]*Department of Astronomy, University of Texas at Austin, Austin, TX 78712, USA*
[4]*Department of Astronomy, School of Science, Kyoto University, Kyoto 606-8502, Japan*

Accepted 2006 December 18. Received 2006 October 5

ABSTRACT

Blazars, a beamed population of active galactic nuclei, radiate high-energy γ-rays, and thus are a good target for the *Gamma Ray Large Area Space Telescope* (*GLAST*). As the blazars trace the large-scale structure of the Universe, one may observe spatial clustering of blazars. We calculate the angular power spectrum of blazars that would be detected by *GLAST*. We show that we have the best chance of detecting their clustering at large angular scales, $\theta \gtrsim 10^\circ$, where shot noise is less important, and the dominant contribution to the correlation comes from relatively low redshift, $z \lesssim 0.1$. The *GLAST* can detect the correlation signal, if the blazars detected by *GLAST* trace the distribution of low-z quasars observed by optical galaxy surveys, which have the bias of unity. If the bias of blazars is greater than 1.5, *GLAST* will detect the correlation signal unambiguously. We also find that *GLAST* may detect spatial clustering of clusters of galaxies in γ-rays. The shape of the angular power spectrum is different for blazars and clusters of galaxies; thus, we can separate these two contributions on the basis of the shape of the power spectrum.

Key words: galaxies: active – BL Lacertae objects: general – galaxies: clusters: general – cosmology: theory – large-scale structure of Universe – gamma-rays: theory.

1 INTRODUCTION

Active galactic nuclei (AGNs) are highly energetic astrophysical objects, which are often accompanied with relativistic jets powered by accretion on to supermassive black holes located at the central region of galaxies. The AGNs radiate in a wide frequency range, from radio waves to γ-rays. The Energetic Gamma Ray Experiment Telescope (EGRET) onboard the *Compton Gamma Ray Observatory* (*CGRO*), which detects γ-rays in GeV energy, have found $\sim$60 AGNs with its all-sky survey campaign, and all of them but one (M87) were classified as 'blazars' (Hartman et al. 1999). The features in the spectrum and light curves of these blazars indicate that the relativistic jets are directed towards us.

The *Gamma Ray Large Area Space Telescope* (*GLAST*) is equipped with the Large Area Telescope (LAT) instrument, which is an upgraded version of the EGRET. Its large effective area (10^4 cm^2) as well as good angular resolution improves the point-source sensitivity by almost two orders of magnitude compared to the EGRET, which would increase the source statistics significantly. It is expected that one thousand to ten thousand blazars would be detected as point sources by *GLAST* (Stecker & Salamon 1996; Chiang & Mukherjee 1998; Mücke & Pohl 2000; Narumoto & Totani 2006). Such a dramatic improvement in point-source sensitivity would allow us to determine the γ-ray luminosity function (GLF) of blazars with unprecedented accuracy. In contrast, the current blazar GLF is based upon merely $\sim$60 blazars detected by EGRET.

As the blazars should trace the large-scale structure of the Universe, they should exhibit spatial clustering. In this paper, we investigate whether the spatial clustering of blazars is detectable by *GLAST*, especially by focusing on the angular power spectrum, a quantity projected along the line of sight. This would provide the first direct measurement of the bias parameter of blazars, immediately after *GLAST* starts taking the data, which should be compared with the results from other classes of AGNs in order to get further insight into the unification picture of AGNs. In addition to blazars, it has been pointed out that *GLAST* may detect γ-ray emission from clusters of galaxies (Colafrancesco & Blasi 1998; Totani & Kitayama 2000). Thus, we also calculate the spatial clustering of clusters of galaxies in γ-rays and discuss its detectability with *GLAST*.

This paper is organized as follows. In Section 2, we calculate the angular power spectrum of blazars that would be detected by *GLAST*. In Section 3, we study detectability of the spatial correlation of blazars and discuss current (indirect) observational constraints on the bias of blazars. In Section 4, we calculate the angular

★E-mail: ando@tapir.caltech.edu

power spectrum of galaxy clusters. Section 5 is devoted to further discussions, and we conclude in Section 6.

2 ANGULAR POWER SPECTRUM OF BLAZARS

2.1 Formalism

The angular power spectrum of blazars that would be detected by *GLAST* is given by the sum of the shot (Poisson) noise term, C_l^P, and the correlation term, C_l^C, as (Peebles 1980)

$$C_l = C_l^P + C_l^C, \tag{1}$$

$$C_l^P = \mathcal{N}^{-1}, \tag{2}$$

$$C_l^C = 2\pi \int_{-1}^{1} \mathrm{d}\cos\theta \; P_l(\cos\theta) w(\theta), \tag{3}$$

where $\mathcal{N} \equiv \mathrm{d}N/\mathrm{d}\Omega$ is the number of blazars per solid angle, and $w(\theta)$ is the angular correlation function of blazars that would be detected by *GLAST*. Note that the shot noise term is independent of multipoles.

A standard procedure to calculate the angular correlation function is as follows. We model the 3D spatial correlation function of blazars, $\xi(r, z)$, as the correlation function of dark matter particles, multiplied by the 'bias' factors that depend on the physics of formation and evolution of blazars in dark matter haloes. We then project the resulting 3D correlation function on the sky to calculate the 2D angular correlation function of blazars, $w(\theta)$. As the bias factors depend on redshift and luminosity of blazars, we model $\xi(r, z)$ as $\xi(r;L_{\gamma,1}, L_{\gamma,2}|z) = \xi_{\rm lin}(r, z)\, b_{\rm B}(L_{\gamma,1}, z)\, b_{\rm B}(L_{\gamma,2},z)$, where $r = |\boldsymbol{x}_2 - \boldsymbol{x}_1|$ is the distance between two blazars, $L_{\gamma,1}$ and $L_{\gamma,2}$ are their luminosities and $\xi_{\rm lin}(r, z)$ is the 3D correlation function of *linear* dark matter fluctuations. As we show in this paper, the angular correlation function of blazars may be detectable only on large scales, and thus the linear correlation function and the linear bias model would provide a good approximation. By projecting the 3D correlation function on the sky, one obtains (Peebles 1980)

$$\mathcal{N}^2 w(\theta) = \int_0^{z_{\rm max}} \mathrm{d}z \; \frac{\mathrm{d}^2 V}{\mathrm{d}z\,\mathrm{d}\Omega} \chi(z)^2 \phi(z)^2 \overline{b}_{\rm B}(z)^2 \times \int_{-\infty}^{\infty} \mathrm{d}u \; \xi_{\rm lin}\left(\sqrt{u^2 + \chi(z)^2\theta^2}, z\right), \tag{4}$$

where $\chi(z)$ is the comoving distance out to an object at z, $\mathrm{d}^2V/\mathrm{d}z\,\mathrm{d}\Omega$ is the comoving volume element per unit solid angle and per unit redshift range, $\overline{b}_{\rm B}(z)$ is the average bias of blazars weighted by the GLF of blazars,[1] $\rho_\gamma(L_\gamma, z)$:

$$\overline{b}_{\rm B}(z) \equiv \frac{1}{\phi(z)} \int_{L_\gamma(F_{\gamma,\rm lim},z)}^{\infty} \mathrm{d}L_\gamma \; \rho_\gamma(L_\gamma, z) b_{\rm B}(L_\gamma, z), \tag{5}$$

and $\phi(z)$ is the cumulative GLF of blazars, i.e. GLF integrated from a given minimum luminosity cut-off,

$$\phi(z) \equiv \int_{L_\gamma(F_{\gamma,\rm lim},z)}^{\infty} \mathrm{d}L_\gamma \; \rho_\gamma(L_\gamma, z). \tag{6}$$

Note that we have not used the so-called 'small-angle approximation' or 'Limber's approximation', as we are mainly interested in the signals on large angular scales, $\theta \gtrsim 10^\circ$.

[1] The luminosity function represents the number of sources per unit comoving volume and unit luminosity range.

We calculate $\xi_{\rm lin}(r, z)$ from the power spectrum of linear matter density fluctuations, $P_{\rm lin}(k)$:

$$\xi_{\rm lin}(r, z) = \int \frac{k^2\,\mathrm{d}k}{2\pi^2} \; P_{\rm lin}(k) \frac{\sin kr}{kr}. \tag{7}$$

We use the linear transfer function given in Eisenstein & Hu (1999) to compute $P_{\rm lin}(k)$.

Equations (2) and (3) suggest that $C_l^P = \mathcal{N}^{-1}$ dominates when the number of blazars detected by *GLAST* is small, making it difficult to detect the correlation term. It is therefore very important to understand how many blazars one can detect with *GLAST*. In the next section, we calculate the expected number count of blazars for *GLAST* using the latest GLF of blazars (Narumoto & Totani 2006).

2.2 Gamma-ray luminosity function of blazars

The basic idea behind the model of the GLF of blazars proposed by Narumoto & Totani (2006) is that the jet activity that powers γ-ray emission from blazars must be related to accretion on to the central black holes, from which X-ray emission emerges; thus, the X-ray and γ-ray luminosity of blazars must be correlated. We use the following relation between GLF of blazars, ρ_γ, and X-ray luminosity function (XLF) of AGNs, $\rho_{\rm X}$:

$$\rho_\gamma(L_\gamma, z) = \kappa \frac{L_{\rm X}}{L_\gamma} \rho_{\rm X}(L_{\rm X}, z). \tag{8}$$

The advantage of this method is that the XLF has been determined accurately by the extensive study of the X-ray background (Ueda et al. 2003; Hasinger, Miyaji & Schmidt 2005), and thus the predicted GLF would also be fairly accurate, provided that the γ-ray luminosity and X-ray luminosity of blazars are tightly correlated. Since not all AGNs detected in X-rays are blazars, we have introduced a normalization factor, κ. We relate the γ-ray luminosity, L_γ, and X-ray luminosity, $L_{\rm X}$, of blazars by a linear relation with the constant of proportionality given by 10^q:

$$L_\gamma = 10^q L_{\rm X}, \tag{9}$$

where L_γ represents νL_ν at 100 MeV, and $L_{\rm X}$ is the X-ray luminosity integrated over the *ROSAT* band, 0.5–2 keV. (Both are evaluated at the source rest frame.) We convert the measured flux to the rest-frame luminosity by specifying the spectrum of sources: for γ-ray we use a spectral index of $\alpha_\gamma = 2.2$ (Sreekumar et al. 1998), while for X-ray $\alpha_{\rm X} = 2$ (Hasinger et al. 2005).

The AGN XLF, $\rho_{\rm X}$, is given by a double power law in luminosity with an evolution factor $f(L_{\rm X}, z)$ (Hasinger et al. 2005):

$$\rho_{\rm X}(L_{\rm X}, z) = \frac{A_{\rm X} f(L_{\rm X}, z)}{(\ln 10) L_{\rm X}} \left[\left(\frac{L_{\rm X}}{L_{\rm X}^*} \right)^{\gamma_1} + \left(\frac{L_{\rm X}}{L_{\rm X}^*} \right)^{\gamma_2} \right]^{-1}, \tag{10}$$

where

$$f(L_{\rm X}, z) = \begin{cases} (1+z)^{p_1} & [z \leqslant z_{\rm c}(L_{\rm X})], \\ f[L_{\rm X}, z_{\rm c}(L_{\rm X})] \left[\frac{1+z}{1+z_{\rm c}(L_{\rm X})} \right]^{p_2} & [z > z_{\rm c}(L_{\rm X})], \end{cases} \tag{11}$$

where $z_{\rm c}$ is the redshift of evolutionary peak given by

$$z_{\rm c}(L_{\rm X}) = \begin{cases} z_{\rm c}^* & (L_{\rm X} \geqslant L_a), \\ z_{\rm c}^* \left(\frac{L_{\rm X}}{L_a} \right)^\alpha & (L_{\rm X} < L_a), \end{cases} \tag{12}$$

and p_1 and p_2 are given by

$$p_1 = p_1^* + \beta_1 \left[\log \left(L_{\rm X}/\mathrm{erg\ s^{-1}} \right) - 44 \right], \tag{13}$$

$$p_2 = p_2^* + \beta_2 \left[\log \left(L_{\rm X}/\mathrm{erg\ s^{-1}} \right) - 44 \right]. \tag{14}$$

Hasinger et al. (2005) have found $A_{\rm X} = 6.69 \times 10^{-7}\,{\rm Mpc}^{-3}$, $\log(L_{\rm X}^*\,{\rm erg\,s^{-2}}) = 43.94 \pm 0.11$, $z_{\rm c}^* = 1.96 \pm 0.15$, $\log(L_a\,{\rm erg\,s^{-2}}) = 44.67$, $\alpha = 0.21 \pm 0.04$, $p_1^* = 4.7 \pm 0.3$, $p_2^* = -1.5 \pm 0.7$, $\beta_1 = 0.7 \pm 0.3$, $\beta_2 = 0.6 \pm 0.8$, $\gamma_2 = 2.57 \pm 0.16$ and $\gamma_1 = 0.87 \pm 0.10$. We call this model the 'luminosity-dependent density evolution' model, LDDE.

How robust are our predictions from this model? The most important parameter for our purpose in this paper is the slope of XLF in the faint end, γ_1, as the expected number count of blazars that would be detected by *GLAST* is sensitive to how many blazars there are in the faint end of luminosity function. Narumoto & Totani (2006) have fitted the GLF of blazars detected by EGRET in order to find γ_1, $q = \log(L_\gamma/L_{\rm X})$ and κ, with the other parameters fixed at the best-fitting values from the XLF given above. (The blazar sample from EGRET was constructed by requiring that EGRET sources were identified as blazars by radio observations. The probability that the blazars giving the flux above the EGRET point-source sensitivity also gives the sufficient radio flux was taken into account in their analysis.) They have found that $(\gamma_1, q, \kappa) = (1.19, 3.80, 5.11 \times 10^{-6})$ best describes the GLF of EGRET blazars. This γ_1 is larger than that obtained from the XLF, $\gamma_1 = 0.87 \pm 0.10$, at the 3σ level, which may imply that a better model is needed; however, we do not investigate this point any further and simply accept $\gamma_1 = 1.19$ as the canonical value for the GLF of blazars. One should come back to this point, however, when *GLAST* flies and collects many more blazars than available now.

One can also calculate the contribution to the extragalactic gamma-ray background (EGRB) from blazars once the GLF is specified. The EGRB intensity has been measured by EGRET (Sreekumar et al. 1998; Strong, Moskalenko & Reimer 2004),[2] and the best-fitting model with $\gamma_1 = 1.19$ accounts for 25–50 per cent of the EGRB intensity, depending on the assumed minimum γ-ray luminosity of blazars, $L_{\gamma,\rm min} = 10^{40}$ to $10^{43}\,{\rm erg\,s^{-1}}$. Here, we assume that no blazars fainter than the minimum luminosity would exist. On the other hand, blazars can still account for all the EGRB intensity, if the blazars can be as faint as $L_{\gamma,\rm min} = 10^{41}\,{\rm erg\,s^{-1}}$, and the faint end of the GLF is slightly steeper, $\gamma_1 = 1.31$, than the canonical model. The other parameters are given by $(q, \kappa) = (3.80, 3.9 \times 10^{-6})$. This model appears to be a bit extreme, as $\gamma_1 = 1.31$ is inconsistent with the X-ray determination, $\gamma_1 = 0.87 \pm 0.10$, at the 4.4σ level. Nevertheless, we use this model to show the uncertainty in our predictions from the uncertainty in the faint end of the GLF. Henceforth, we call the canonical model ($\gamma_1 = 1.19$) the 'LDDE1' model, and the latter model ($\gamma_1 = 1.31$) the 'LDDE2' model. For both models, we adopt $L_{\gamma,\rm min} = 10^{41}\,{\rm erg\,s^{-1}}$ as the lower luminosity cut-off.

2.3 Survey parameters, number count, angular correlation function and power spectrum of blazars from *GLAST*

The flux sensitivity for point sources of the *GLAST* LAT is $F_{\gamma,\rm lim} = 2 \times 10^{-9}\,{\rm cm^{-2}\,s^{-1}}$ for 2 yr of full-sky observations and for sources having the energy spectral index of 2; we adopt this value of the flux sensitivity in the following discussions, unless otherwise stated. The γ-ray flux, F_γ, represents the flux integrated above $E_{\rm min} = 100\,{\rm MeV}$, and it is related to the γ-ray luminosity through

$$L_\gamma(F_\gamma, z) = \frac{4\pi d_{\rm L}^2(\alpha_\gamma - 1)}{(1+z)^{2-\alpha_\gamma}} E_{\rm min} F_\gamma, \tag{15}$$

[2] But these estimates are still controversial (Keshet, Waxman & Loeb 2004b).

Table 1. Parameters of the LDDE GLFs and the expected number, N, and the surface number density, $\mathcal{N}$, of blazars that would be detected by *GLAST*. We have assumed that no blazars fainter than $L_{\gamma,\rm min} = 10^{41}\,{\rm erg\,s^{-1}}$ would exist, and *GLAST* LAT can detect the flux down to $F_{\gamma,\rm lim} = 2 \times 10^{-9}\,{\rm cm^{-2}\,s^{-1}}$ for 2 yr of all-sky observations.

Model	(q, γ_1)	κ	N	$\mathcal{N}\,({\rm sr^{-1}})$
LDDE1[a]	(3.80, 1.19)	5.11×10^{-6}	3100	250
LDDE2[b]	(3.80, 1.31)	3.90×10^{-6}	6500	520

[a] Best-fitting model of the EGRET blazar distribution.
[b] A model explaining 100 per cent of the EGRB intensity.

where $d_{\rm L}$ is the luminosity distance. One can calculate the number of blazars that would be detected by *GLAST* from

$$N = \Omega \int_0^{z_{\rm max}} {\rm d}z\, \frac{{\rm d}^2 V}{{\rm d}z\,{\rm d}\Omega} \phi(z), \tag{16}$$

where we use $z_{\rm max} = 5$, Ω is the solid angle covered ($\Omega = 4\pi$ sr for the all-sky survey) and $\phi(z)$ is the cumulative GLF given by equation (6).

For the canonical GLF model that accounts for 25–50 per cent of the EGRB intensity (LDDE1) and the lower luminosity cut-off of $L_{\gamma,\rm min} = 10^{41}\,{\rm erg\,s^{-1}}$ (hereafter, we use this value unless otherwise stated), we obtain $N \simeq 3100$. For the GLF model that accounts for all the EGRB intensity (LDDE2) and the same luminosity cut-off, we obtain $N \simeq 6500$. These results are summarized in Table 1. Therefore, it is easier to detect the spatial clustering of blazars in the LDDE2 model than in the LDDE1 model.

Fig. 1 shows the redshift distribution of *GLAST* blazars predicted from the LDDE1 and LDDE2 model. For both cases, the distribution exhibits a sharp cut-off around $z = 0.01$, which is due to our assumption that no blazars fainter than $L_{\gamma,\rm min}$ would exist; a

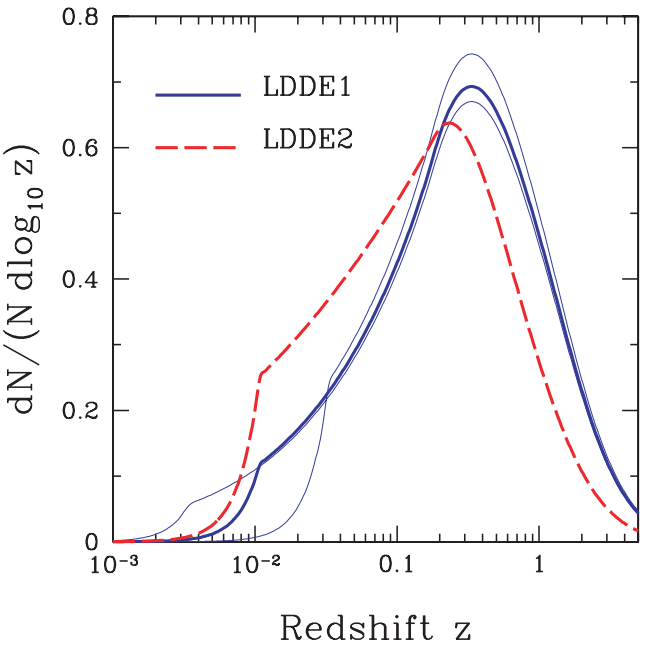

Figure 1. Redshift distribution of blazars that would be detected by *GLAST*, for LDDE1 (solid) and LDDE2 (dashed) models. (See Table 1 for the model parameters as well as for the expected number of blazars.) The thick solid line shows the LDDE1 model with $L_{\gamma,\rm min} = 10^{41}\,{\rm erg\,s^{-1}}$, while the thin solid lines show the LDDE1 model with $L_{\gamma,\rm min} = 10^{40}\,{\rm erg\,s^{-1}}$ and $10^{42}\,{\rm erg\,s^{-1}}$: the larger the $L_{\gamma,\rm min}$ is, the fewer the low-z blazars would be detected.

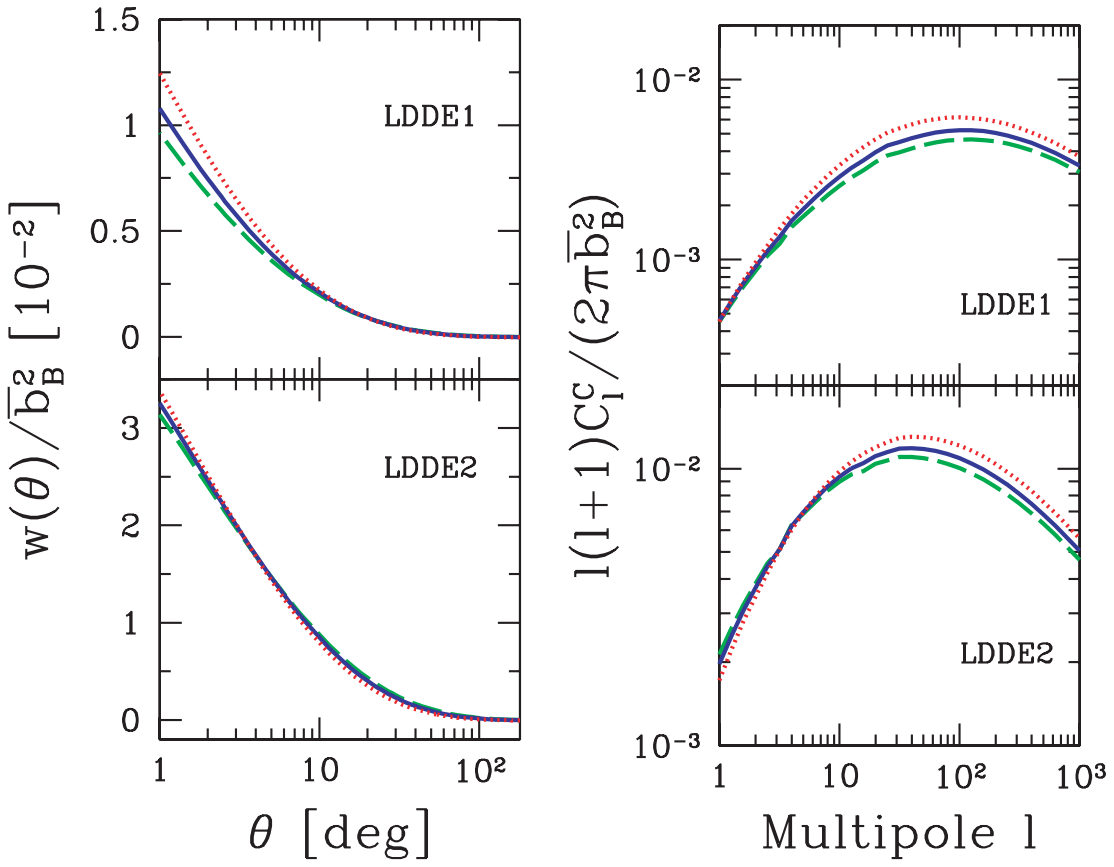

Figure 2. Angular correlation function (left-hand side), $w(\theta)$, and (right-hand side) correlation term of the angular power spectrum, $l(l+1)C_l^C/2\pi$, of the blazars that would be detected by *GLAST*. Both have been divided by the average bias squared; thus plotted quantities are $w(\theta)/\overline{b}_B^2$ and $l(l+1)C_l^C/(2\pi\overline{b}_B^2)$. The dotted, solid and dashed lines show the predictions for the limiting flux of $F_{\gamma,\rm lim} = 2$, 3 and 4×10^{-9} cm^{-2} s^{-1}, respectively. The top panels are for the LDDE1 model, while the bottom panels are for the LDDE2 model.

larger $L_{\gamma,\rm min}$ results in a larger cut-off redshift. Nevertheless, since only a small fraction of the distribution is eliminated by this effect, the total number of blazars that would be detected by *GLAST*, N, hardly changes; for example, we expect 3200 and 2900 blazars to be observed by *GLAST* for $L_{\gamma,\rm min} = 10^{40}$ and 10^{42} erg s^{-1} (both for the LDDE1 parameters), respectively. On the other hand, we will show in Section 3.1 that $L_{\gamma,\rm min}$ has an important consequence for detectability of the anisotropy signal.

Fig. 2 shows the angular correlation function, $w(\theta)$ (left-hand panels), and the correlation term of the angular power spectrum, $l(l+1)C_l^C/2\pi$ (right-hand panels), divided by the average bias squared, for the LDDE1 (top panels) and LDDE2 (bottom panels) model. In each panel, we vary the *GLAST* LAT point-source flux sensitivity, $F_{\gamma,\rm lim}$, from 2×10^{-9} to 4×10^{-9} cm^{-2} s^{-1}. As expected, the clustering is stronger when more sources are observed, i.e. LDDE2 and lower $F_{\gamma,\rm lim}$.

3 DETECTABILITY OF THE BLAZAR CORRELATION

3.1 Signal-to-noise versus blazar bias

As the correlation function and power spectrum are proportional to the average bias squared, $w(\theta) \propto \overline{b}_B^2$ and $C_l^C \propto \overline{b}_B^2$, whether or not one can detect the angular clustering of blazars crucially depends on $\overline{b}_B$. Before we investigate a model of the blazar bias, let us ask this question, 'how large $\overline{b}_B$ should be, in order for C_l^C to be detected by *GLAST*?'

The statistical error in the measurement of C_l is given by the following argument. Assuming statistical isotropy of the Universe, we have $2l+1$ independent samples of $C_l = |a_{lm}|^2$ (with different m) per multipole. Here, a_{lm} is the spherical harmonic coefficient of the distribution of blazars on the sky. One may thus estimate C_l from $C_l = \sum_{m=-l}^{l} |a_{lm}|^2/(2l+1)$. The error in C_l is given by

$$(\delta C_l)^2 = \frac{2C_l^2}{(2l+1)\Delta l f_{\rm sky}} = \frac{2(C_l^P + C_l^C)^2}{(2l+1)\Delta l f_{\rm sky}}, \qquad (17)$$

where Δl is the bin size in l space and $f_{\rm sky}$ is a fraction of the sky covered by observations. For the all-sky survey like *GLAST*, we may adopt $f_{\rm sky} = 1$; we note that the point-source sensitivity becomes worse near the Galactic plane because of strong Galactic foreground. As $C_l^P = \mathcal{N}^{-1}$ is independent of l and depends only on the inverse of the surface density of blazars, one can fit it and subtract it from the measured C_l, leaving only C_l^C. The error in C_l^C, however, still contains the contribution from C_l^P. This shows why it is important to detect as many blazars as possible (and thus reduce C_l^P as much as possible), in order to measure C_l^C.

Fig. 3 shows the 1σ error boxes binned with $\Delta l = 0.5l$ for the LDDE1 and LDDE2 model. We show the errors for the average bias of $\overline{b}_B = 1$ and 3. (Note that we have ignored the redshift dependence of $\overline{b}_B$.) We find that it would be difficult to detect C_l^C for the LDDE1

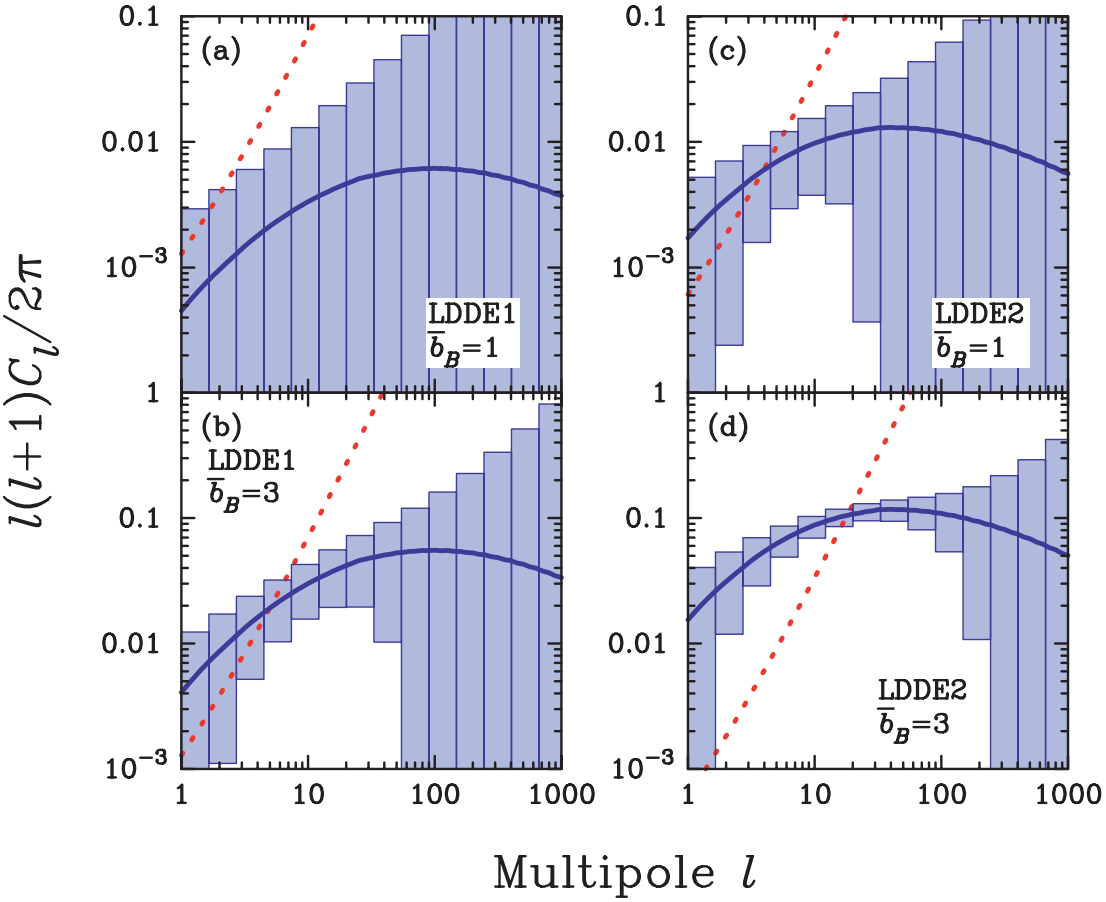

Figure 3. Angular power spectrum of *GLAST* blazars, $l(l+1)C_l/2\pi$. The dotted lines show the shot noise term, C_l^P (equation 2), while the thick solid lines show the correlation term, C_l^C (equation 3), for the following models: (a) LDDE1, $\overline{b}_B = 1$, (b) LDDE1, $\overline{b}_B = 3$, (c) LDDE2, $\overline{b}_B = 1$ and (d) LDDE2, $\overline{b}_B = 3$. The boxes show the 1σ errors in C_l^C binned with $\Delta l = 0.5l$ (equation 17).

plus $\overline{b}_B = 1$ model, while the other models yield sufficient signal-to-noise ratios.

To increase statistical power, one may sum C_l over multipoles. Let us define the angular power spectrum averaged over $2 \leqslant l \leqslant 30$,[3]

$$\overline{C}(2 \leqslant l \leqslant 30) = \frac{1}{29}\sum_{l=2}^{30} C_l. \tag{18}$$

The errors of this quantity are then given by

$$(\delta\overline{C})^2 = \sum_{l=2}^{30}\left(\frac{\partial\overline{C}}{\partial C_l}\right)^2 [\delta C_l(\Delta l = 1)]^2$$
$$= \frac{1}{29^2}\sum_{l=2}^{30}\frac{2}{(2l+1)f_{\rm sky}}\left(C_l^P + C_l^C\right)^2. \tag{19}$$

Fig. 4 shows $\overline{C}^C(2 \leqslant l \leqslant 30)$ as a function of the average blazar bias, $\overline{b}_B$, for the LDDE1 (top panel) and LDDE2 (bottom panel) models. The expected 1σ errors as well as the Poisson contribution, $\overline{C}^P$, are also shown. For the LDDE1 model, we find that *GLAST* can detect $\overline{C}^C$ if $\overline{b}_B \gtrsim 1.2$. For the LDDE2 model, the detection is much easier, even for $\overline{b}_B \gtrsim 0.5$.

[3] A dipole component, C_1, depends on Earth's motion and is not considered here.

Our results depend on the luminosity cut-off of the GLF, $L_{\gamma,\rm min}$, as the correlation at large separations ($l \lesssim 30$) is dominated mainly by relatively nearby (less bright) sources. We have therefore performed the same calculations with different $L_{\gamma,\rm min}$ (with the other parameters of the LDDE1 model held fixed), and found that the correlation would be detectable (i.e. $\overline{C}^C/\delta\overline{C} > 1$) for the average bias greater than 0.9 and 1.7, for $L_{\gamma,\rm min} = 10^{40}$ and 10^{42} erg s^{-1}, respectively.

One may also ask how these results would change, if we chose other GLF models. The 'pure-luminosity evolution' (PLE) model has been used traditionally in the literature (Stecker & Salamon 1996; Chiang & Mukherjee 1998), while the LDDE model fits the EGRET blazar properties better (Narumoto & Totani 2006). Motivated by the correlation between radio and γ-ray luminosities of blazars, Stecker & Salamon (1996) used the PLE model to obtain the GLF of blazars. We find that the large-angle correlation ($l \leqslant 30$) is more difficult to detect in their model: the correlation would be detectable only when $\overline{b}_B > 4.2$. Their model, however, was not intended to reproduce the redshift and luminosity distributions of the EGRET blazars, and thus their fit to these data is not very good. Chiang & Mukherjee (1998) improved the PLE model by adjusting a few parameters such that the model can reproduce the distribution of EGRET blazars. [Although the authors did not use the radio and γ-ray luminosity relation, we incorporate this in our calculations (see Narumoto & Totani 2006 for details).] Again, we find that the correlation signal is more difficult to detect

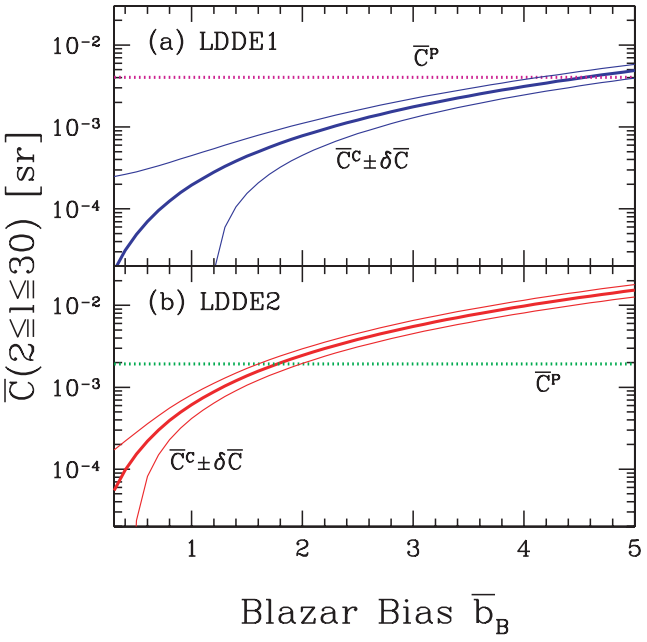

Figure 4. Angular power spectrum averaged over $2 \leqslant l \leqslant 30$, $\overline{C}$ (equation 18), as a function of the average bias of blazars. The dotted lines show the Poisson term, $\overline{C}^P$, while the thick solid lines show the correlation term, $\overline{C}^C$, for (a) LDDE1 and (b) LDDE2. The thin solid lines show the 1σ errors in $\overline{C}^C$ (equation 19).

in the best-fitting PLE model: the correlation would be detectable only when $\overline{b}_B > 6.9$. These results are because the PLE model predicts the blazar distribution that is much more biased towards the high redshift [see fig. 11 of Narumoto & Totani (2006)], and hence, the large-separation power (due mainly to low-z blazars) is suppressed. In fact, the results improve if we instead adopt the smaller separation, $30 \leqslant l \leqslant 300$, where the high-$z$ contribution becomes larger. The sensitivity to the bias parameter goes down to $\overline{b}_B > 2.4$ and $\overline{b}_B > 3.0$, respectively, for the Stecker & Salamon (1996) and Chiang & Mukherjee (1998) models. On the other hand, as we have already shown, the latest GLF from the LDDE model, which best describes the distribution of EGRET blazars, predicts that the correlation would be detectable for $\overline{b}_B$ of order of unity.

3.2 Modelling blazar bias

The bias of blazars is not known, and thus *GLAST* may provide the first determination of the blazar bias, if it is greater than 1.2 (for LDDE1; 0.5 for LDDE2). In this section, we estimate the blazar bias from the existing observations using three different (indirect) techniques: the bias of quasars, X-ray observations and halo model. However, we emphasize that none of these estimates can be very accurate (and in fact, they disagree each other) – we will need *GLAST* to give us the answer.

3.2.1 Bias from optical quasar surveys

If the blazar is truly a beamed population of AGNs, then its bias should be correlated with that of AGNs observed in other wavebands. It is therefore natural to use such information to estimate the bias of blazars.

The optical quasar surveys, such as the Two-degree Field Quasar Redshift Survey and the Sloan Digital Sky Survey (SDSS), may be the most efficient way for doing this. Fig. 5(a) shows the spectroscopic result that the Two-degree Field Quasar Redshift Survey suggests (Croom et al. 2005)

$$b_Q(z) = 0.56 + 0.289(1+z)^2, \tag{20}$$

which is also consistent with the photometric result from the SDSS (Myers et al. 2006). By comparing $b_Q(z)$ with the bias of dark matter haloes (which is discussed later), Croom et al. (2005) found that the mass of dark matter haloes that host quasars is typically $\sim 4 \times 10^{12}\,M_\odot$, almost independent of redshift.

In order to make a quantitative comparison between the results obtained here and those in the previous section, we define an 'effective bias', $b_B^{\rm eff}(l)$, by

$$b_B^{\rm eff}(l) = \sqrt{\frac{C_l[\text{model bias}, \overline{b}_B(z)]}{C_l(\overline{b}_B = 1)}}, \tag{21}$$

where the numerator is C_l^C calculated with $\overline{b}_B(z) = b_Q(z)$, and the denominator is that calculated with $\overline{b}_B = 1$. If $b_B^{\rm eff}(l)$ is greater than 1.2 and 0.5 for the LDDE1 and LDDE2 models, respectively, *GLAST* can detect C_l^C from this population. The top curves of Fig. 6 show $b_B^{\rm eff}(l)$ as a function of l. We find that $b_B^{\rm eff}(l) \sim 0.8$ for a relevant range of multipoles; thus, C_l^C is detectable for the LDDE2 model but not for the LDDE1 model. We also find that $b_B^{\rm eff}(l)$ increases as l does (haloes at higher redshifts are contributing more to the small angular scales), although the dependence is only modest and is not able to bring the bias to high enough values for detection for the LDDE1 model.

Since the multipole l is roughly related to the angular separation via $\theta \approx 180^\circ/l$, the angular power spectrum at $l \sim 10$ contributes most to the angular correlation function, $w(\theta)$, at $\theta \approx 20^\circ$. In Fig. 5(b), we show that the contribution to $w(\theta)$ per $\log z$ peaks at

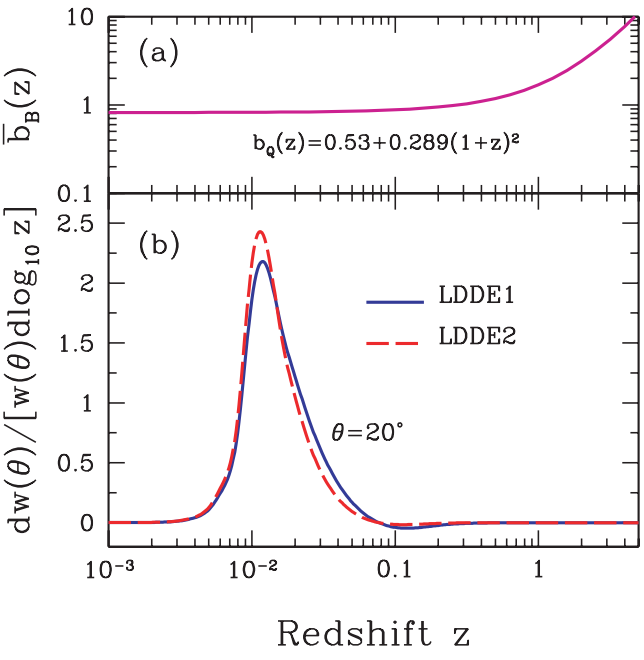

Figure 5. (a) Quasar bias, $b_Q(z)$, from the Two-degree Field Quasar Redshift Survey, and (b) contribution to the angular correlation function per $\log z$, $\mathrm{d}\,w(\theta)/[w(\theta)\,\mathrm{d}\log z]$, at $\theta = 20^\circ$, for the LDDE1 (solid) and LDDE2 (dashed) models. We have used $b_Q(z)$ for the average blazar bias, $\overline{b}_B(z)$.

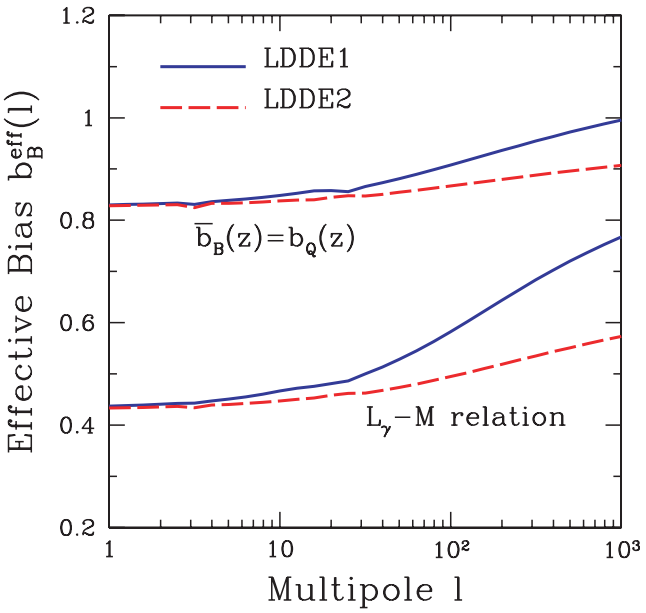

Figure 6. The effective bias, $b_{\rm B}^{\rm eff}(l)$, for the LDDE1 (solid) and LDDE2 (dashed) models. The top curves are from $\overline{b}_{\rm B}(z) = b_{\rm Q}(z)$, while the bottom curves are from the halo model with L_γ–M relation (equation 22).

$z \sim 0.01$ with a tail extending up to $z \sim 0.1$. At such low redshifts, the value of the averaged bias is $\sim$0.8, almost independent of z.

3.2.2 *Bias from X-ray point-source surveys*

The GLF proposed by Narumoto & Totani (2006) that we are using in this paper was derived on the basis of a correlation between γ-ray and X-ray luminosities of emission from blazars. Therefore, the bias derived from the spatial clustering of AGNs detected in X-ray surveys may provide a useful information regarding the bias of blazars.

Nevertheless, the clustering of AGNs determined from X-ray surveys is somewhat controversial. While both the angular and 3D correlation function of the X-ray bright AGNs detected by the *ROSAT* surveys are consistent with those from the optical quasar surveys (Vikhlinin & Forman 1995; Mullis et al. 2004), those from *Chandra* and *XMM–Newton* suggest that these sources are clustered more strongly than optically selected quasars (Yang et al. 2003; Basilakos et al. 2005; Gandhi et al. 2006). The latest determination of $w(\theta)$ from the *XMM–Newton* Large Scale Structure Survey gave $w(30\,\mathrm{arcsec}) \sim 0.2$ for approximately 1130 sources detected over 4.2 deg^2 on the sky in the 0.5–2 keV band (Gandhi et al. 2006), although statistical significance is only $\sim 2\sigma$. This result may be interpreted as the bias being $\sim$3.7 (or $\lesssim$3.7 at the 2σ level), which we have obtained as follows: using the LDDE XLF and the best-fitting parameters in Hasinger et al. (2005), we have calculated $w(\theta)$ from equation (4), in which we have used the spatial correlation function of *non-linear* dark matter fluctuations, as non-linearity cannot be ignored at such a small angular separation. [We have used the halo model approach (Seljak 2000) to obtain the non-linear power spectrum.] If such a large bias is realized also for blazars, then *GLAST* should quite easily be able to detect the correlation. We should, however, keep in mind that no significant correlations were observed in the 2–10 keV band, and one needs to improve the source statistics before making any definitive conclusion about the bias of AGNs from X-ray surveys.

3.2.3 *Bias from halo model*

Finally, we try to estimate the bias of blazars from the halo model. As any galaxies (hosting blazars) must form in dark matter haloes, the bias of blazars should be related to the bias of dark matter haloes, $b_{\rm h}(M, z)$, which is known accurately from N-body simulations as well as from analytical models such as the extended Press–Schechter model (e.g. Mo & White 1996). Let us suppose that the γ-ray luminosity of blazars is correlated with the mass of host dark matter haloes, $L_\gamma = L_\gamma(M_{\rm h})$. Then, the bias of blazars may be estimated from the bias of dark matter haloes via $b_{\rm B}(L_\gamma, z) = b_{\rm h}[M_{\rm h}(L_\gamma), z]$. We use $b_{\rm h}[M_{\rm h}(L_\gamma), z]$ derived by Mo & White (1996).

The relation between the γ-ray luminosity of blazars and the host halo mass is not known. Whether or not such a relation actually exists is not known either. Moreover, even if there is a relation between L_γ and $M_{\rm h}$, not all haloes would host blazars, especially when one takes into account the fact that the jets from blazars should be directed towards us. We nevertheless estimate $b_{\rm B}$ here using the following argument. Since it is plausible that the blazar γ-rays are emitted via the inverse-Compton scattering of the relativistic electrons accelerated in blazar jets off the cosmic microwave background (CMB), the γ-ray luminosity would be correlated with the activity of a central supermassive black hole. Wang, Staubert & Ho (2002) have found an empirical relation between the blazar luminosity at the peak frequency (i.e. a frequency at which the blazar emits most energy, νL_ν), $L_{\rm pk}$, in the optical to X-ray regime and the luminosity of emission lines, $L_{\rm lines}$, in the optical. The line luminosity is related to the Eddington luminosity via $\log(L_{\rm lines}/L_{\rm Edd}) \approx -5$ to -3 (Wang et al. 2002) which, in turn, would give a $L_{\rm pk}$–$M_{\rm BH}$ relation, where $M_{\rm BH}$ is a black hole mass which determines the Eddington luminosity. We then relate the γ-ray luminosity, L_γ, with the peak luminosity, $L_{\rm pk}$, by assuming that they are roughly equal, $L_\gamma \approx L_{\rm pk}$ (Inoue & Takahara 1996; Kataoka et al. 1999). We still need to relate the black hole mass, $M_{\rm BH}$, with the host halo mass, $M_{\rm h}$, for which we use a correlation between the black hole mass and the host *galaxy* mass, M (Ferrarese et al. 2006). Of course, the galaxy mass may not be equal to the dark halo mass, the latter being larger, as dark matter haloes extend more than the luminous part of galaxies. We find that this uncertainty hardly affects our prediction for the blazar bias. Using these arguments, we finally obtain the desired relation,

$$M = 10^{11.3}\,\mathrm{M}_\odot \left(\frac{L_\gamma}{10^{44.7}\ \mathrm{erg\ s^{-1}}}\right)^{1.7}, \qquad (22)$$

for $\log(L_{\rm lines}/L_{\rm Edd}) = -4$. We will use this relation for estimating the blazar bias from $b_{\rm B}(L_\gamma, z) = b_{\rm h}[M(L_\gamma), z]$.

Before we proceed further, let us address the uncertainty in our treatment. If we used $\log(L_{\rm lines}/L_{\rm Edd}) = -3$ instead of -4, and $L_\gamma = 0.1 L_{\rm pk}$ instead of $L_\gamma = L_{\rm pk}$, we would obtain $M = 10^{13}\,\mathrm{M}_\odot\,(L_\gamma/10^{44}\ \mathrm{erg\ s^{-1}})^{1.7}$, making the host haloes more massive and hence the larger bias for the same luminosity. We find, however, that the resulting $\overline{b}_{\rm B}$ did not change significantly.

Fig. 7(a) shows $\overline{b}_{\rm B}(z)$ from equation (5) with $b_{\rm B}(L_\gamma, z) = b_{\rm h}[M(L_\gamma), z]$ and equation (22). Fig. 7(b) shows that the most dominant contribution to $w(\theta)$ at $\theta = 20^\circ$ comes from $z \lesssim 0.1$, which implies that the angular power spectrum of blazars that would be detected by *GLAST* would have the average bias of about 0.4, which is too small for *GLAST* to measure C_l^C. Both LDDE1 and LDDE2 give very similar results. The reason why we found such a small bias

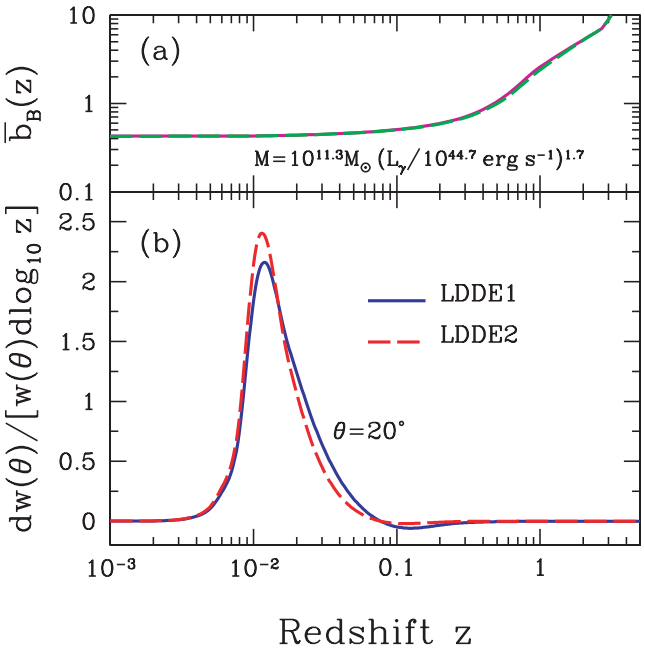

Figure 7. The same as Fig. 5, but for the blazar bias equal to the bias of dark matter haloes with an empirical γ-ray luminosity–mass relation (equation 22).

is that our model predicts that *GLAST* would detect fainter blazars at low redshifts than bright galaxies at high redshifts. Therefore, the average bias is dominated by the faint, low-z blazars that have a small bias. (Faint blazars are formed in low-mass dark matter haloes, which have a small bias.) At $z \gtrsim 0.5$, on the other hand, $\overline{b}_B(z)$ can be as larger as unity, as only the bright blazars (in massive haloes) are detectable.

Although it does not affect our analysis very much, let us mention one subtle feature of the halo approach we just described. The GLF of blazars may be related to the mass function of dark matter haloes, dn_h/dM_h, as

$$dL_\gamma\ \rho_\gamma(L_\gamma, z) = dM_h\ \frac{dn_h}{dM_h}(M_h, z) N_B(M_h, z), \tag{23}$$

where $N_B(M_h, z)$ is the so-called 'halo occupation distribution', which represents the average number of blazars per each halo of mass, M_h, at a given redshift, z. One can use this relation, GLF (ρ_γ), and L_γ–M_h relation to obtain $N_B(M_h, z)$. Using the Press–Schechter function (Press & Schechter 1974) for dn_h/dM_h and the LDDE1 model for ρ_γ, we have found that $N_B(M, z)$ diverges exponentially at the high-mass end. This is because dn_h/dM_h has an exponential cut-off, while ρ_γ given by the LDDE1 model decreases only as a power law with the luminosity. Of course, this divergence is an artefact from the fact that we do not know the precise shape of the GLF at the brightest end, which is poorly constrained. It is likely that (i) the GLF has a maximum luminosity above which it rapidly approaches zero, and (ii) the assumed L_γ–M relation cannot be extrapolated to large luminosities. In order to remove the divergence, we have put an upper cut-off in the GLF so that $N_B(M, z)$ never exceeds 1. For the LDDE1 model, the cut-off luminosity is 3×10^{47} erg s^{-1}, which keeps the GLF still consistent with the EGRET data because the contribution to the GLF from such luminous blazars is not significant [see fig. 12 of Narumoto & Totani (2006)].

Any of the assumptions we have made in this section could be incorrect. The *GLAST* data will provide us with much better idea about the clustering of blazars, which will enable us to test these assumptions.

4 ANGULAR POWER SPECTRUM OF GALAXY CLUSTERS

4.1 Gamma-ray emission from galaxy clusters

There is a fascinating possibility that *GLAST* finds clusters of galaxies in γ-rays (Berezinsky, Blasi & Ptuskin 1997; Colafrancesco & Blasi 1998; Loeb & Waxman 2000; Totani & Kitayama 2000; Waxman & Loeb 2000; Keshet et al. 2003; Miniati 2003; Keshet, Waxman & Loeb 2004a). A fraction of the EGRB may be due to these clusters of galaxies. While no convincing detection has been made so far from EGRET (Reimer et al. 2003), there are a few reports of marginal evidence for a correlation between the position of galaxy clusters and the EGRET data (Kawasaki & Totani 2002; Scharf & Mukherjee 2002). In fact, there are many EGRET unidentified sources whose positions are coincident with Abell clusters or high galaxy density regions, but the physical association cannot be established because of low statistics and large EGRET error circles. It is expected that *GLAST* will give us the first conclusive evidence for γ-ray emission from galaxy clusters.

Clusters of galaxies may emit γ-ray via two processes. One is the collision between relativistic protons accelerated by shock waves and surrounding cold matter, mainly protons, producing neutral pions which decay into γ-rays. Since protons hardly lose their energy by radiative loss and their diffusion time is much longer than the age of the Universe, all the clusters are expected to emit some γ-rays by this mechanism (Berezinsky et al. 1997; Colafrancesco & Blasi 1998). The other mechanism is the inverse-Compton scattering of relativistic electrons off the CMB photons (Loeb & Waxman 2000; Totani & Kitayama 2000; Waxman & Loeb 2000; Keshet et al. 2003; Miniati 2003; Keshet et al. 2004a). As for the source of these relativistic electrons, the most popular scenario is that the shocks associated with the formation of large-scale structure accelerate electrons to relativistic speed. In the following sections, we will explore these two possibilities and calculate the angular power spectrum that would be measured by *GLAST*.

4.1.1 Proton–proton collisions

The cumulative luminosity function, $\phi(z)$ (equation 6), for the cluster γ-ray emission from proton–proton collisions is given by

$$\phi_{C,pp}(z) = \int_{M_h(F_{\gamma,\mathrm{lim}},z)}^{\infty} dM_h\ \frac{dn_h}{dM_h}(M_h, z), \tag{24}$$

where we label quantities regarding clusters by attaching the subscript C henceforth; another subscript *pp* means that the γ-ray emission comes originally from the proton–proton (*pp*) collisions.

In order to relate the γ-ray flux to the halo mass and redshift, $M_h(F_\gamma, z)$, we follow the model of Colafrancesco & Blasi (1998): relativistic protons are injected from the very central region of clusters, in which the central AGN or cD galaxy powers such an injection. These protons then diffuse from the central region to outside with the efficiency that is determined by the magnetic field strength. We assume that a fraction, $\epsilon_B = 10^{-3}$, of the baryon energy is given to the magnetic energy. For proton energies of our interest, the diffusion time-scale is always longer than the age of the Universe; thus, protons are always confined within clusters. Using the radial injection profile of these diffused protons as well as the density

Table 2. Model parameters, α and ϵ, the expected number count, N, the surface density, $\mathcal{N}$, the average bias, $\overline{b}_{\rm C}(z = 0.01)$, of clusters that would be detected by *GLAST*. The last column lists the expected signal-to-noise ratio for detecting the correlation power spectrum averaged over $2 \leqslant l \leqslant 30$.

Model	$\alpha_{\rm p,e}$	$\epsilon_{\rm p,e}$	N	$\mathcal{N}$ (sr^{-1})	$\overline{b}_{\rm C}$	$\overline{C}^C/\delta\overline{C}$
*pp*1	2.2	0.5	6600	530	2.0	7.0
*pp*2	2.2	0.1	1100	88	2.5	4.6
*pp*3	2.2	0.01	63	5.0	3.3	1.9
IC1	2	0.05	3700	290	1.4	4.5
IC2	2	0.01	430	34	1.7	2.4
IC3	2.2	0.01	62	4.9	2.2	1.3

profile of the surrounding medium that is well measured in X-rays, one can compute the rate of *pp* collisions. The efficiency of the γ-ray production from each collision is given in Kelner, Aharonian & Bugayov (2006), which we follow in our calculation. We use a power law with an index of $\alpha_{\rm p} = 2.2$ for the proton spectrum, with an upper cut-off whose energy is determined by a balance between the diffusion time-scale and the cluster age (Colafrancesco & Blasi 1998). (We found that the cut-off energy is much larger than the energy scale of our interest.)

We calculate the total energy of relativistic protons, $E_{\rm p}$, by assuming that a fraction, $\epsilon_{\rm p}$, of the gravitational binding energy of baryons is given to protons, i.e. $E_{\rm p} = \epsilon_{\rm p} E_{\rm b} \approx \epsilon_{\rm p}(\Omega_{\rm b}/\Omega_{\rm m}) M V_{\rm c}^2$, where $V_{\rm c}$ is the circular velocity at the virial radius, and adopt three values for $\epsilon_{\rm p} = 0.5$ (*pp*1), 0.1 (*pp*2) and 0.01 (*pp*3). Note that the equipartition model, *pp*1, has been excluded marginally by observations (Blasi 1999); however, we keep this model as an upper bound on the γ-ray emission from clusters of galaxies via proton–proton collisions. The other two models (*pp*2 and *pp*3) are allowed by observations. The most pessimistic cases, *pp*3 and IC3, are in agreement with the estimates given in Gabici & Blasi (2004). We summarize the parameters of these models as well as the expected number of clusters that would be detected by *GLAST* in Table 2. We find that a large number of galaxy clusters are expected to be seen in the *GLAST* data, which would provide an exciting possibility of investigating the physics of galaxy clusters using γ-ray observations. Fig. 8(a) shows the redshift distribution of clusters that would be detected by *GLAST* with these models.

4.1.2 *Inverse-Compton scattering*

Since electrons lose their kinetic energy via radiation loss rapidly compared with the dynamical time of clusters of galaxies, γ-ray emission would emerge only near the formation of shocks. The cumulative luminosity function, $\phi(z)$ (equation 6), for the cluster γ-ray emission from the inverse-Compton scattering is thus given by (Totani & Kitayama 2000)

$$\phi_{\rm C,IC}(z) = \int_{M_{\rm h}(F_{\gamma,\rm lim},z)}^{\infty} {\rm d}M_{\rm h}\; R_{\rm form}(M_{\rm h}, z)\Delta t_{\gamma}, \qquad (25)$$

where $R_{\rm form}(M_{\rm h}, z)$ is the formation rate of clusters with mass of $M_{\rm h}$ at z, per comoving volume, and Δt_{γ} is the time-scale during which γ-rays are radiated efficiently from each cluster. We calculate Δt_{γ} as either the inverse-Compton cooling time or the shock wave propagation time (whichever is longer): $\Delta t_{\gamma} = \max\{t_{\rm IC}, t_{\rm shock}\}$. In most cases of our interest, the latter is always much longer than the former, and therefore, $\Delta t_{\gamma} = t_{\rm shock} \simeq r_{\rm vir}/v_{\rm s} = 1.5(1+z)^{-3/2}$ Gyr, independent of $M_{\rm h}$, where $r_{\rm vir}$ is the virial radius and $v_{\rm s}$ the sound speed. The formation rate of clusters, $R_{\rm form}(M_{\rm h}, z)$, is given by the time-derivative of the halo mass function, ${\rm d}n_{\rm h}/{\rm d}M_{\rm h}(M_{\rm h}, z)$, corrected for the halo destruction rate (Kitayama & Suto 1996).

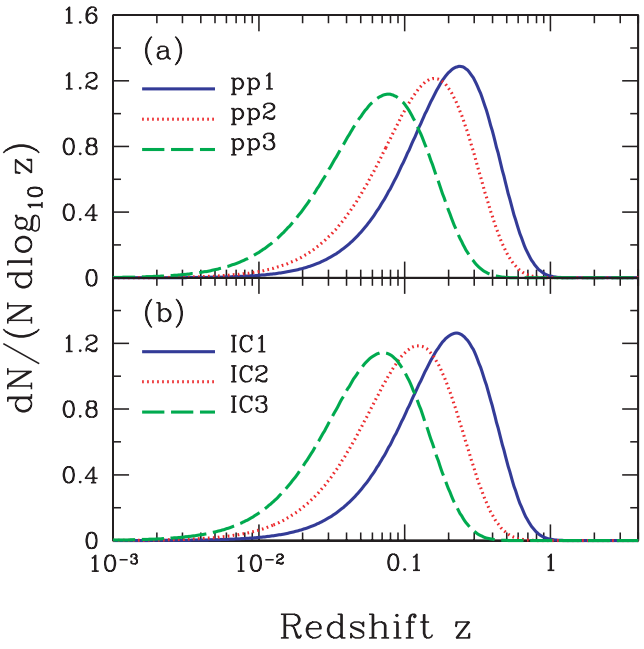

Figure 8. Redshift distribution of clusters of galaxies that would be detected by *GLAST* for (a) proton–proton collision and (b) inverse-Compton scattering models. Model parameters are given in Table 2.

Similar to the proton–proton collision case, we calculate the total energy of relativistic electrons, $E_{\rm e}$, by assuming that a fraction, $\epsilon_{\rm e}$, of the gravitational binding energy of baryons is given to electrons. We use a power law with an index of $\alpha_{\rm e}$ (either 2 or 2.2; see Table 2) for the γ-ray spectrum, with an upper cut-off whose energy is determined by a balance between the acceleration time-scale and the cooling time-scale. To calculate the acceleration time-scale, we use the magnetic field energy given by $\epsilon_{\rm B} = 10^{-3}$ times the binding energy of baryons. We choose $(\alpha_{\rm e}, \epsilon_{\rm e}) = (2, 0.05)$, $(2, 0.01)$ and $(2.2, 0.01)$ as our models, and we call them IC1, IC2 and IC3, respectively. The IC1 model is investigated by Totani & Kitayama (2000), and it gives maximally allowed number of γ-ray emitting clusters, as the IC1 model predicts the EGRB flux that is as large as what is measured by EGRET. These models are again summarized in Table 2 and Fig. 8.

4.2 Angular power spectrum of galaxy clusters from *GLAST*

The angular power spectrum of clusters of galaxies[4] is given by equations (1)–(4) with the averaged blazar bias, $\overline{b}_{\rm B}$, replaced by the average cluster bias,

$$\overline{b}_{{\rm C},pp}(z) = \frac{1}{\phi_{{\rm C},pp}(z)} \int_{M_{\rm h}(F_{\gamma,\rm lim},z)}^{\infty} {\rm d}M_{\rm h}\; \frac{{\rm d}n_{\rm h}}{{\rm d}M_{\rm h}}(M_{\rm h}, z)\, b_{\rm h}(M_{\rm h}, z), \qquad (26)$$

$$\overline{b}_{\rm C,IC}(z) = \frac{1}{\phi_{\rm C,IC}(z)} \int_{M_{\rm h}(F_{\gamma,\rm lim},z)}^{\infty} {\rm d}M_{\rm h}\; R_{\rm form}(M_{\rm h}, z)\Delta t_{\gamma}\, b_{\rm h}(M_{\rm h}, z), \qquad (27)$$

[4] Waxman & Loeb (2000), followed by Keshet et al. (2003, 2004a), studied the angular correlation of the radio and γ-ray background radiation from galaxy clusters.

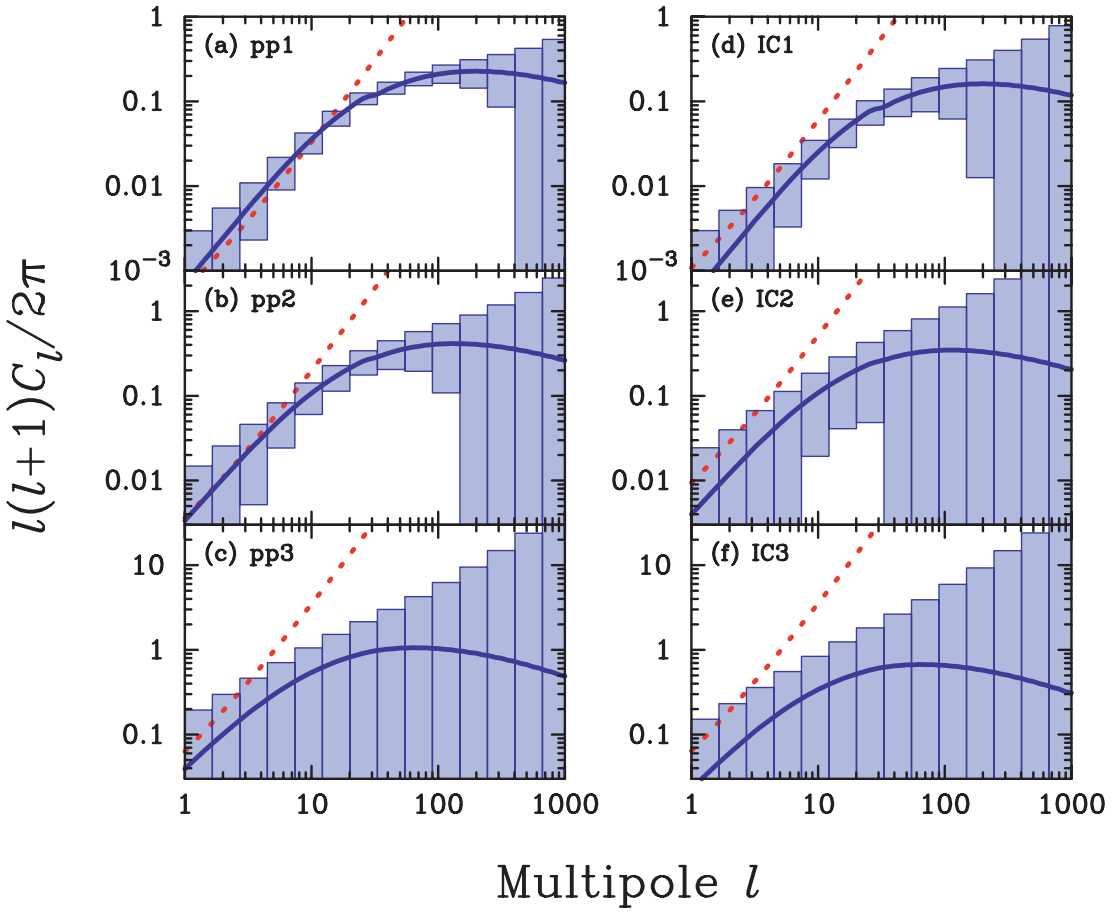

Figure 9. The same as Fig. 3 but for galaxy clusters. The left-hand panels show the proton–proton collision models (*pp*1, *pp*2, *pp*3), while the right-hand panels show the inverse-Compton models (IC1, IC2, IC3) (see Table 2 for the model parameters).

for the proton–proton collision model and the inverse-Compton model, respectively.

Fig. 9 shows the angular power spectrum of these γ-ray clusters with the binned error boxes ($\Delta l = 0.5l$) as well as the shot noise term for (a)–(c) proton–proton collision and (d)–(f) inverse-Compton models. The correlation is quite significant particularly for optimistic models predicting large number of γ-ray emitting clusters being detected by *GLAST*, i.e. *pp*1 and IC1. The last column of Table 2 shows the signal-to-noise ratio for the power spectrum averaged over $2 \leqslant l \leqslant 30$, $\overline{C}/\delta\overline{C}$. We find that the signal-to-noise ratio exceeds unity for all the models that we have considered: the minimum is $\overline{C}/\delta\overline{C} = 1.3$ for IC3, and the maximum is 7.0 for *pp*1, despite the fact that only small number of clusters are expected to be seen in the *GLAST* data. This is because clusters of galaxies are formed in the high-density peaks and thus are highly biased. The sixth column of Table 2 shows the average bias factors of clusters at $z = 0.01$.

5 DISCUSSION

5.1 Admixture of blazars and galaxy clusters

While follow-up programs should reveal the identity of the *GLAST* γ-ray sources and also some of the galaxy clusters might appear as extended sources, at a very early stage of *GLAST* observational campaign, all the point sources should more generally be considered to be mixed of various emitters. Here, we consider two-population case, blazars and galaxy clusters. Our purpose in this section is to investigate whether it is possible to distinguish the blazar component from that of clusters by the angular clustering, even before the follow-ups.

When there are more than one species of sources on the sky, one should also consider cross-correlation between different species. When there are blazars and galaxy clusters in the γ-ray sky, the angular power spectrum is given by

$$C_l = C_{l,\mathrm{B}} + C_{l,\mathrm{C}} + 2C_{l,\mathrm{BC}}, \tag{28}$$

where $C_{l,\mathrm{B}}$ and $C_{l,\mathrm{C}}$ are the spectra from blazars (Section 2) and clusters (Section 4), respectively. The surface number density of sources in this case is instead given by the sum of the two species, $\mathcal{N} = \mathcal{N}_\mathrm{B} + \mathcal{N}_\mathrm{C}$. The last term, $C_{l,\mathrm{BC}}$, represents the cross-correlation between blazars and galaxy clusters, and is given by

$$C_{l,\mathrm{BC}} = 2\pi \int_{-1}^{1} \mathrm{d}\cos\theta \; P_l(\cos\theta) w_\mathrm{BC}(\theta), \tag{29}$$

$$\mathcal{N}^2 w_\mathrm{BC}(\theta) = \int_0^{z_\mathrm{max}} \mathrm{d}z \; \frac{\mathrm{d}^2 V}{\mathrm{d}z\,\mathrm{d}\Omega} \chi(z)^2 \phi_\mathrm{B}(z)\phi_\mathrm{C}(z)\overline{b}_\mathrm{B}(z)\overline{b}_\mathrm{C}(z) \times \int_{-\infty}^{\infty} \mathrm{d}u \; \xi_\mathrm{lin}(\sqrt{u^2 + \chi(z)^2\theta^2}, z), \tag{30}$$

where $\phi_\mathrm{B}(z)$ (equation 6) and $\phi_\mathrm{C}(z)$ (equations 24 or 25) as well as

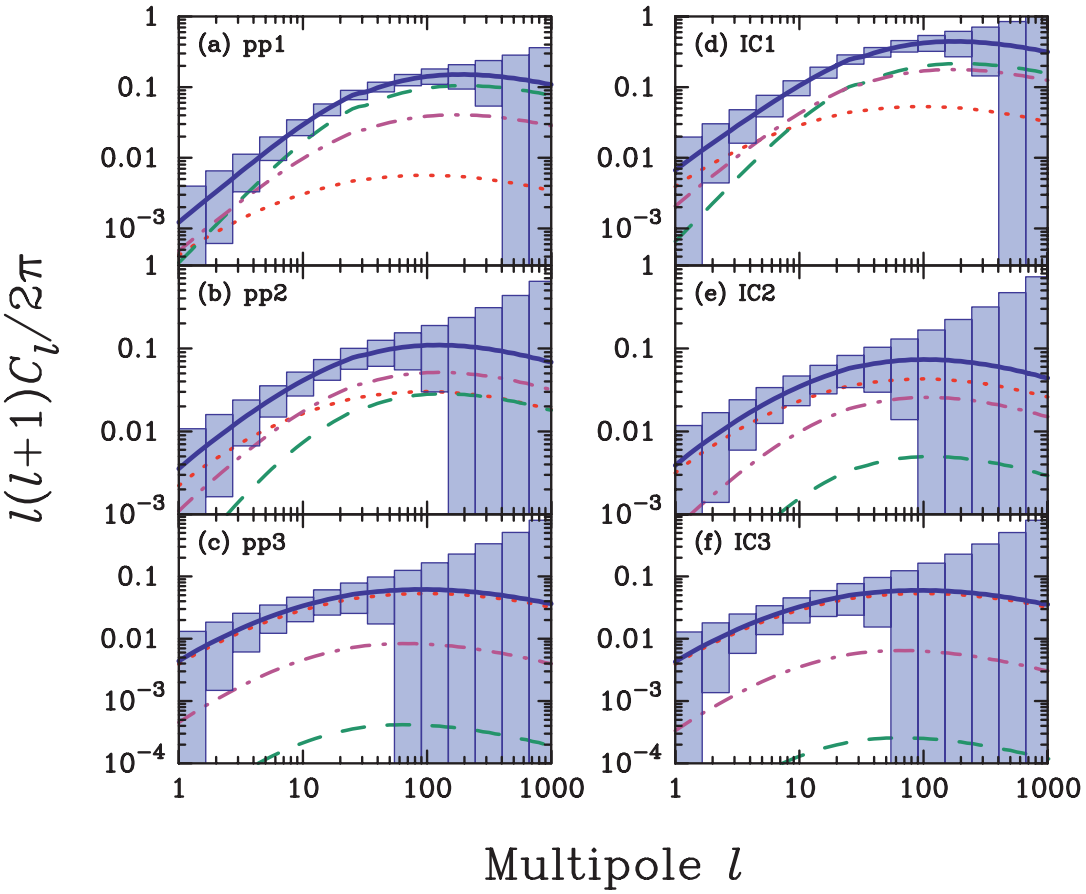

Figure 10. Angular power spectrum of blazars for the LDDE1 model with $\overline{b}_{\rm B} = 3$ (dotted), clusters of galaxies (dashed) and cross-correlation between blazars and clusters (dot–dashed). The thick solid curves show the total signal, $C_l^C = C_{l,\rm B}^C + C_{l,\rm C}^C + 2C_{l,\rm BC}$, while the boxes show the binned errors ($\Delta l = 0.5l$). The left-hand panels show the proton–proton collision models ($pp1, pp2, pp3$), while the right-hand panels show the inverse-Compton models (IC1, IC2, IC3) (see Table 2 for the model parameters).

$\overline{b}_{\rm B}(z)$ (equation 5) and $\overline{b}_{\rm C}(z)$ (equations 26 or 27) have been given in the previous sections.

Fig. 10 shows the angular power spectrum of *GLAST* point sources, including blazars (LDDE1 and $\overline{b}_{\rm B} = 3$) and galaxy clusters for various models. If the average blazar bias is as large as 3, the power spectrum from blazars almost always dominates the signal, especially at low l. An interesting feature in Fig. 10 is that the shape of blazar power spectrum and cluster spectrum is quite distinct: the cluster spectrum falling towards low multipoles more rapidly than the blazar spectrum (i.e. the cluster spectrum rising towards high multipoles more rapidly than the blazar spectrum). Therefore, when the blazar signal dominates ($pp3$ and IC3 in Fig. 10), one would see a shallower power spectrum, while when the cluster signal dominates ($pp1$ and IC1), one would see a steeper power spectrum at $l \lesssim 30$. This feature may help us identify the dominant source of clustering seen by *GLAST*. We do not know which point sources *GLAST* would detect, blazars or clusters, until the follow-up observations are carried out; however, the angular power spectrum may provide us with useful information regarding the dominant species.

5.2 Identifying *GLAST* point sources with radio survey

The Faint Images of the Radio Sky at Twenty Centimeters (FIRST) survey (Becker, White & Helfand 1995) has detected ∼811 k radio sources over 9033 square deg^2, or ∼90 sources per square degree, with the source detection threshold of 1 mJy at 1.4 GHz.[5] Since many of the *GLAST* point sources will be within the FIRST field of view, the FIRST survey will provide us with valuable information regarding identification of the point sources that would be detected by *GLAST*.

How bright are blazars and galaxy clusters in radio? The EGRET blazar catalogue was constructed such that the EGRET sources are also detected in radio. The correlation between radio and γ-ray luminosities of blazars is not yet well understood, and there is a considerable dispersion (Mücke et al. 1997). However, the standard synchrotron self-Compton model of blazars predicts that there should be some correlation. Narumoto & Totani (2006) assumed a proportional relation between mean radio luminosity, $L_{\rm r}$, and L_γ, with a dispersion obeying to the lognormal distribution, and found that mean relation of $L_{\rm r} = 10^{-3.23} L_\gamma$ and dispersion $\sigma[\log\,(L_{\rm r}/L_\gamma)] = 0.49$ fitted the observed data well. Using this relation and assuming that the spectral index in radio is given by $\alpha_{\rm r} = 1.0$ (because the radio emission is due to synchrotron radiation), we find that the flux in radio that corresponds to the limiting flux for the point sources that can be detected by *GLAST* in γ-rays is given by $F_{\rm r,GLAST,lim} = (1+z)^{2-\alpha_{\rm r}}(10^{-3.23}L_\gamma)/(4\pi d_{\rm L}^2) = 10^{-3.23}(1+z)^{\alpha_\gamma-\alpha_{\rm r}}(\alpha_\gamma - 1)E_{\rm min}F_{\gamma,\rm lim}$, where we have used equation (15). We thus find $F_{\rm r,GLAST,lim} \sim 10$ mJy, which is an order

[5] http://sundog.stsci.edu/first

of magnitude brighter than the limiting flux for the point sources detected by the FIRST survey.[6] Therefore, we expect the radio counterparts for the *GLAST* blazars to be found in the existing FIRST point-source catalogue (if they are within the FIRST field of view), although some sources which deviate from the L_r–L_γ relation above may be missed.

The radio emission from galaxy clusters is also likely from synchrotron radiation. For the inverse-Compton scenario, one can estimate the luminosity in radio from a ratio of the CMB and magnetic field energy density, in which case the radio luminosity from galaxy clusters is much smaller than that expected from blazars having the same γ-ray luminosity (Totani & Kitayama 2000). For the proton–proton collision scenario, they would be even dimmer in radio; otherwise they should also be detectable by γ-rays due to the electron inverse-Compton scattering. Therefore, unlike blazars, galaxy clusters would not be identifiable with the FIRST survey, which makes the FIRST survey a good diagnosis tool for the identification of the *GLAST* point sources.

5.3 Measuring blazar anisotropy with *GLAST*

Based upon the results that we have obtained so far, we here show one example strategy for the point-source survey and identification of blazars that would be carried out by *GLAST*.

(i) *Source detection.* After its launch, *GLAST* will start detecting γ-ray sources from all the directions on the sky. Some of them would be extended sources (such as nearby galaxy clusters), and some would be highly variable (such as γ-ray bursts). These sources should be removed.

(ii) *Removing galaxy clusters.* As blazars are also bright in radio but galaxy clusters are not, one may remove galaxy clusters from the *GLAST* data using the source catalogue from the FIRST survey (Section 5.2).

(iii) *Updating GLF and further cut.* With the *GLAST* source catalogue from (ii), which would consist mostly of blazars, one may update the GLF of blazars by extending it down to fainter sources than those that EGRET has detected. At this point, we probably gain some insight as to which GLF model fits the data better, LDDE1 or LDDE2, or whether or not we need a different GLF model. If LDDE1 is indeed confirmed, then one needs other populations of sources in order to explain the bulk of EGRB.

(iv) *Analysis of angular power spectrum.* Measure the angular power spectrum of the sources that have survived the cuts in (i) and (ii). Since we have currently several models which predict a variety of the blazar bias, from 0.4 to 4 (Section 3.2), the power spectrum measured at $l \lesssim 30$ should provide us with useful information regarding the blazar bias. While we would expect the contribution from galaxy clusters is minimal in this catalogue owing to the cuts in (i) and (ii), the shape of the power spectrum would also provide useful (albeit indirect) confirmation that the bulk of the sources in the catalogue are blazars. The blazar bias measured from *GLAST*, or an upper limit on the bias, would be the first direct measurement of the bias of blazars, which would shed light on the formation process of blazars and their link to the quasars detected in the optical and the AGNs detected in X-rays.

(v) *Completion of follow-ups: beginning of precision study.* When the source identification with direct follow-up observations is complete, one should revisit the blazar source catalogue, establish the GLF of blazars more firmly and re-analyse the angular power spectrum. At this point, it would also be possible to obtain the 3D power spectrum, as opposed to the angular spectrum, using the redshift information from follow-up observations. This would be very powerful in constraining the formation and evolution of blazars, as one can constrain the evolution of blazar bias as a function of redshift, provided that enough number of blazars are detected by *GLAST*.

[6] The luminosities at 1.4 and 2.7 GHz are the same, as we adopt $\alpha_r = 1$.

6 CONCLUSIONS

In this paper, we have calculated the angular power spectrum of blazars and galaxy clusters that would be detected by *GLAST*. We have shown that *GLAST* can detect the spatial clustering of blazars if the average bias of blazars exceeds 1.2 and 0.5, for the canonical GLF model (LDDE1) that accounts for 25–50 per cent of the extragalactic γ-ray background (EGRB) and the extreme model (LDDE2) that accounts for all the EGRB, respectively (Narumoto & Totani 2006). While the blazar bias is not known with any precision, current observations seem to suggest, albeit indirectly, that it can take on any values between $\sim$0.4 and $\sim$4; thus, the *GLAST* data will provide us with the first, direct estimate of the bias of blazars which, in turn, would constrain the formation and evolution of blazars.

As for galaxy clusters, which are highly biased objects, we have found that the signal-to-noise ratio of the correlation exceeds unity for all the models we have considered (Table 2): proton–proton collisions followed by pion decay (Berezinsky et al. 1997; Colafrancesco & Blasi 1998), and inverse-Compton scattering of relativistic electrons off CMB (Loeb & Waxman 2000; Totani & Kitayama 2000; Waxman & Loeb 2000; Keshet et al. 2003; Miniati 2003; Keshet et al. 2004a).

We have shown that the angular power spectra of blazars and galaxy clusters are quite distinct at low multipoles, $l \lesssim 30$, the blazar spectrum being much shallower than the cluster one. This feature helps us identify the population dominating the angular power spectrum of the point sources that would be detected by *GLAST*.

Although the full follow-up observations would take a long time, a quick (but less accurate) identification of sources is possible with the existing FIRST survey data in radio at 1.4 GHz, as most of the blazars should also be bright enough to be seen in radio, while galaxy clusters should not. We have given an example strategy for using the angular power spectrum as a diagnosis tool for blazars in Section 5.3.

With an impressive number of blazars as well as galaxy clusters expected to be detected by *GLAST*, one should maximize the scientific outcome from the *GLAST* data by using as many tools as possible. The angular power spectrum (or angular correlation function) is easy to calculate from the point-source catalogue, and would give us invaluable information about the spatial clustering of blazars and high-energy activity in clusters of galaxies, which are poorly known at present.

ACKNOWLEDGMENTS

SA and EK would like to thank Jennifer Carson for useful discussion; SA is also grateful to Andrew Benson and Marc Kamionkowski for comments. SA was supported by Sherman Fairchild Fellowship at Caltech. EK acknowledges support from an Alfred P. Sloan Foundation. TN and TT were supported by a Grant-in-Aid for the 21st Century COE 'Centre for Diversity and Universality in Physics'

from the Ministry of Education, Culture, Sports, Science and Technology of Japan.

REFERENCES

Basilakos S., Plionis M., Georgakakis A., Georgantopoulos I., 2005, MNRAS, 356, 183
Becker R. H., White R. L., Helfand D. J., 1995, ApJ, 450, 559
Berezinsky V. S., Blasi P., Ptuskin V. S., 1997, ApJ, 487, 529
Blasi P., 1999, ApJ, 525, 603
Chiang J., Mukherjee R., 1998, ApJ, 496, 752
Colafrancesco S., Blasi P., 1998, Astropart. Phys., 9, 227
Croom S. M. et al., 2005, MNRAS, 356, 415
Eisenstein D. J., Hu W., 1999, ApJ, 511, 5
Ferrarese L. et al., 2006, ApJ, 644, L21
Gabici S., Blasi P., 2004, Astroparticle Phys., 20, 579
Gandhi P. et al., 2006, A&A, 457, 393
Hartman R. C. et al., 1999, ApJS, 123, 79
Hasinger G., Miyaji T., Schmidt M., 2005, A&A, 441, 417
Inoue S., Takahara F., 1996, ApJ, 463, 555
Kataoka J. et al., 1999, ApJ, 514, 138
Kawasaki W., Totani T., 2002, ApJ, 576, 679
Kelner S. R., Aharonian F. A., Bugayov V. V., 2006, Phys. Rev. D, 74, 034018
Keshet U., Waxman E., Loeb A., Springel V., Hernquist L., 2003, ApJ, 585, 128
Keshet U., Waxman E., Loeb A., 2004a, ApJ, 617, 281
Keshet U., Waxman E., Loeb A., 2004b, J. Cosmology Astroparticle Phys., 04, 006
Kitayama T., Suto Y., 1996, MNRAS, 280, 638
Loeb A., Waxman E., 2000, Nat, 405, 156
Miniati F., 2003, MNRAS, 342, 1009
Mo H. J., White S. D. M., 1996, MNRAS, 282, 347
Mullis C. R., Henry J. P., Gioia I. M., Böhringer H., Briel U. G., Voges W., Huchra J. P., 2004, ApJ, 617, 192
Mücke A., Pohl M., 2000, MNRAS, 312, 177
Mücke A. et al., 1997, A&A, 320, 33
Myers A. D. et al., 2006, ApJ, 638, 622
Narumoto T., Totani T., 2006, ApJ, 643, 81
Peebles P. J. E., 1980, The Large-Scale Structure of the Universe. Princeton Univ. Press, Princeton, NJ
Press W. H., Schechter P., 1974, ApJ, 187, 425
Reimer O., Pohl M., Sreekumar P., Mattox J. R., 2003, ApJ, 588, 155
Scharf C. A., Mukherjee R., 2002, ApJ, 580, 154
Seljak U., 2000, MNRAS, 318, 203
Sreekumar P. et al., 1998, ApJ, 494, 523
Stecker F. W., Salamon M. H., 1996, ApJ, 464, 600
Strong A. W., Moskalenko I. V., Reimer O., 2004, ApJ, 613, 956
Totani T., Kitayama T., 2000, ApJ, 545, 572
Ueda Y., Akiyama M., Ohta K., Miyaji T., 2003, ApJ, 598, 886
Vikhlinin A., Forman W., 1995, ApJ, 455, L109
Wang J.-M., Staubert R., Ho L. C., 2002, ApJ, 579, 554
Waxman E., Loeb A., 2000, ApJ, 545, L11
Yang Y., Mushotzky R. F., Barger A. J., Cowie L. L., Sanders D. B., Steffen A. T., 2003, ApJ, 585, L85

This paper has been typeset from a TEX/LATEX file prepared by the author.